JOURNAL OF MATERIALS SCIENCE **40** (2005) 155–164

Durability of YZA ceramic foams in a porous burner

P. J. ELVERUM, J. L. ELLZEY, D. KOVAR
Department of Mechanical Engineering, University of Texas at Austin, Austin, TX 78712, USA
E-mail: dkovar@mail.utexas.edu

The durability of YZA cellular ceramic foams was investigated in the demanding environment of an instrumented porous burner. Following exposure to the combustion environment, the ceramic foam coupons suffered moderate damage. Coupons exposed to extended duration tests in the burner did not show additional damage compared to coupons exposed to short duration tests indicating that damage occurred during start-up, when temperature gradients were most severe. To compare the results of the burner tests to conventional thermal shock experiments, samples were also exposed to a water quench test. Coupons removed from the burners and coupons exposed to the water quench from high temperatures exhibited similar failure morphologies. In both cases a marked transition in failure morphology was observed as the magnitude of the peak temperatures and thermal gradients were increased. Chemical analysis combined with these thermal shock measurements show that damage sustained by the foams in the burner results from thermal shock and not from chemical degradation.

1. Introduction

Radiant burners and gas turbine combustors can be constructed such that the combustion process takes place within the open cells of a metallic or ceramic foam [1, 2]. Heat transfer from the flame is enhanced through both conduction and radiation due to the presence of the connected solid. Because the incoming gases are preheated, lean flames may be stabilized over a range of flow velocities [3–5] resulting in low emissions of CO, NO_x and unburned hydrocarbons [6, 7]. In addition, the porous burner offers other advantages such as more uniform temperature and flame velocity profiles that are beneficial in gas turbine combustors.

Burners operating on premixed fuel and air must have some means of stabilizing the flame at a fixed location and preventing the propagation of the flame into the upstream piping. Extensive research on porous burners has shown that a burner consisting of two sections of cellular foam media, an upstream section with small cells and a downstream section of larger cells, stabilizes the flame over a range of conditions [2, 6, 8, 9]. The smaller cells prevent the propagation of the flame into the upstream section and thus provides the safety characteristics necessary for a premixed burner.

The temperature gradient in these burners is quite severe. The upstream face of the porous burner is typically at ambient temperature. The peak temperature occurs in the downstream section and is dependent upon the operating conditions. Due to material limitations, the maximum temperature is typically less than 1800 K. The thermal gradient depends on the properties of the porous sections but values of 500 to 1000 K/cm are typical in porous burners [9]. Due to their higher melting temperature, oxidation resistance, and superior creep resistance [10], ceramic foams offer potentially improved performance over metallic foams for combustion applications. However, because of low fracture toughness and poor thermal conductivity, and the extreme temperature gradients that exist in a porous burner, the primary concern in the use of ceramics for burners has been their durability [1, 2, 7].

In fully dense ceramics, the propagation of a single crack can cause catastrophic failure of an entire component. In contrast, the propagation of a crack in ceramic foams causes failure of individual struts, but damage is not catastrophic because the struts are isolated from each other by the continuous open cells [11]. Ceramic foams, therefore, exhibit greater damage tolerance compared to fully dense monolithic ceramics. Nevertheless, the fracture of several adjacent struts can lead to failure of a section of material and, in extreme cases, the ejection of ceramic material from the foam. In addition to degrading the performance of the burner, fracture of struts and the ejection of material are detrimental because of the potential for contaminating downstream components. Other potential problems for ceramics in burners include possible chemical reactions between unstable constituents within the ceramic foam or between the foam and the combustion products that could degrade the mechanical strength of the foams.

The purpose of this work is to assess the durability of a YZA ceramic foam in a porous burner and to

elucidate the failure mechanisms of ceramic foams exposed to combustion. Based on preliminary experiments with a variety of ceramic foams, yttria-stabilized zirconia/alumina composites (YZA) have shown the greatest promise in burners [12]. YZA foam burners were tested under realistic combustion conditions in a burner. Following burner testing, the ceramic foam coupons were removed from the burner and examined to determine whether chemical changes or changes in phase composition had occurred. A second set of coupons was also tested in the burner and their compressive strength was measured to determine the extent to which the foams were damaged by exposure to the combustion environment. For comparison, a third group of ceramic foam coupons was exposed to a water quench from elevated temperature and then tested in compression to assess thermal shock resistance.

2. Experimental procedure

2.1. Materials and characterization

YZA ceramic foams were obtained from Porvair Corp. (Hendersonville, NC) in the form of right cylinders with a height and diameter of approximately 50 mm. According to the manufacturer, the struts within the foam consisted of a mixture of yttria-stabilized zirconia and alumina. Foams with two cell sizes, designated by the manufacturer as 3.9 pores per centimeter (ppc) and 23.6 ppc, were selected for all of the tests conducted in this study. The corresponding average cell sizes for these materials were 2 mm and 250 μm, respectively. The bulk density of the foams was calculated by dividing the nominal volume of the coupons by the mass. The relative density was calculated by dividing the bulk density by the density of the strut material.

Because of the visible variability in cell shape and cell size, additional measurements were made on individual coupons by sectioning, mounting, and polishing. The digitized optical micrographs were then examined using a commercial image analysis program (Clemex Vision, Longueil, Quebec, Canada). For the 23.6 ppc foam, micrographs were taken from 5 different coupons to obtain a representative area for these measurements. For the 3.9 ppc foam, 10 different coupons were used to measure a representative number of cells.

Chemical changes due to exposure to the combustion environment were assessed by examining selected coupons in a scanning electron microscope (SEM) equipped with energy dispersive spectroscopy (EDS) prior to and after testing. The phase composition of each of the foams was determined by pulverizing both an as-received coupon and a coupon removed from the burner and then examining each using X-ray diffraction (XRD) to determine if any changes had occurred as a result of exposure to the combustion environment.

2.2. Burner tests

A schematic of the burner is shown in Fig. 1. This design, consisting of two sections of cellular media, is used in the current study due to its flame stability characteristics [2, 5, 6, 8, 9]. This design is also attractive from the standpoint that the flame, and thus the temperature gradient, is maintained at a fixed location within the burner once the burner is operating at steady-state.

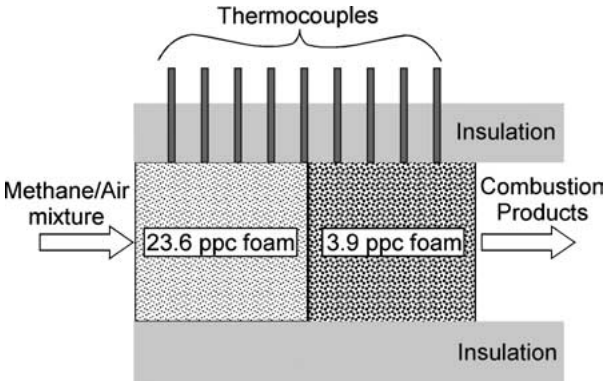

Figure 1 A schematic of the burner design.

Although details about the design and operation of the burner are described elsewhere [9], a brief summary is presented here. The porous burner consisted of two stacked cylindrical ceramic coupons encapsulated in an insulating sleeve. The upstream coupon was made from the 23.6 ppc foam while the downstream coupon was made from the 3.9 ppc foam. A row of thermocouples was located at 1.27 cm intervals along the length of the coupons to measure the position of the flame and the temperature at the interface between the coupons and insulation. A pre-mixed flow of methane and air was used as the fuel source with the flow velocities controlled using mass flow controllers. A range of flow velocities and fuel/air ratios were examined. The fuel to air ratio is specified in terms of an equivalence ratio, ϕ, which is the ratio of methane to air, normalized to the stoichiometric ratio. Thus, ϕ equal to 1 implies

$$CH_4 + 2O_2 \rightarrow CO_2 + 2H_2O \quad (1)$$

Values of ϕ less than 1 imply that the burner was being run "lean" (i.e., excess oxygen was supplied).

In an effort to minimize variations in temperature during start-up, a standard start-up procedure was adopted. After calibrating the emission analyzers, the air and methane mass flow controllers were set to the desired flow velocities and equivalence ratio. Once the flow velocities had stabilized, the burner was ignited at the downstream end of the 3.9 ppc foam. Over a period of approximately 5 min, the flame then migrated completely through the 3.9 ppc coupon, eventually stabilizing near the interface between the two coupons. During operation of the burner, the flame front was approximately planar, with the front parallel to the interface between the foams. After the test was completed, the fuel/air mixture was shut off and the coupons were allowed to cool under ambient conditions.

After each test, the foam coupons were removed and replaced and the tests were repeated 4 or 5 times for each condition. Burner tests were conducted using one of three sets of conditions. For burner condition 1, the equivalence ratio was set to 0.65, the flow rate was set to 30 cm/s, and the duration of the test after the flame stabilized was 30 min. For burner condition 2, the equivalence ratio was set to 0.72 and the flow rate was set to 40 cm/s, and the duration of the test was

30 min. For burner condition 3, the equivalence ratio was set to 0.70, the flow rate was set to 40 cm/s, and the duration of the test was 240 min.

2.3. Water quench tests

Coupons with the same size and geometry as those used in the burner tests were used to assess thermal shock resistance of the foams using a water quench test. Although there are several difficulties that arise in directly analyzing temperature gradients when materials containing open porosity are exposed to a water quench, there currently are no other standardized methods for assessing thermal shock in ceramic foams. Further, the thermal shock resistance of other ceramic foams have been assessed using this method [13] allowing comparison of the current results on YZA foams to previous results on other foam materials. To conduct the quench tests, samples were heated in a tube furnace and then allowed to equilibrate at a given temperature for approximately 10 min before being dropped into a bath containing approximately 20 liters of water at room temperature. Coupons were quenched from temperatures of 490, 690, 890, and 1090 K.

2.4. Mechanical testing

Coupons, in the as-received state, following burner testing, or after a water quench were tested in compression to determine the extent to which they were damaged by burner testing or the water quench. Coupons were placed in an articulating compression fixture lined with 3 mm thick neoprene pads to distribute the load at the contact points between the coupons and the fixtures, as suggested by Dam *et al.* [14]. Tests were conducted using a computer-controlled testing frame at a crosshead displacement rate of 0.5 mm/s. Load and crosshead displacement were measured and the engineering stress and engineering strain were calculated based on the nominal dimensions of the coupons.

TABLE I Characterization of the ceramic foam materials from measurements of bulk density and from stereographic measurements made on sectioned coupons

Bulk density			Stereographic		
Material (ppc)	Pore (%)	Strut (%)	Intrastrut porosity (%)	Interstrut porosity (%)	Strut (%)
3.9	88.9	11.1	1.91	85.2	12.9
23.6	86.4	13.6	1.50	82.9	15.6

3. Results

3.1. Materials characterization

A photograph of the as-received, cylindrical coupons is shown in Fig. 2 and cross-sections of the foams at higher magnifications are shown in Fig. 3a–b. From these micrographs it is clear that the foams consist of a large fraction of open cells and a much smaller fraction of ceramic struts. The open cells are approximately equiaxed and do not exhibit significant directionality. A summary of the structural measurements for the foams is presented in Table I. The measured average bulk density based on the volume and mass is 0.605 g/cm^3 (11.1%) for the 3.9 ppc foam and 0.744 g/cm^3 (13.6%) for the 23.6 ppc. The stereographic analysis

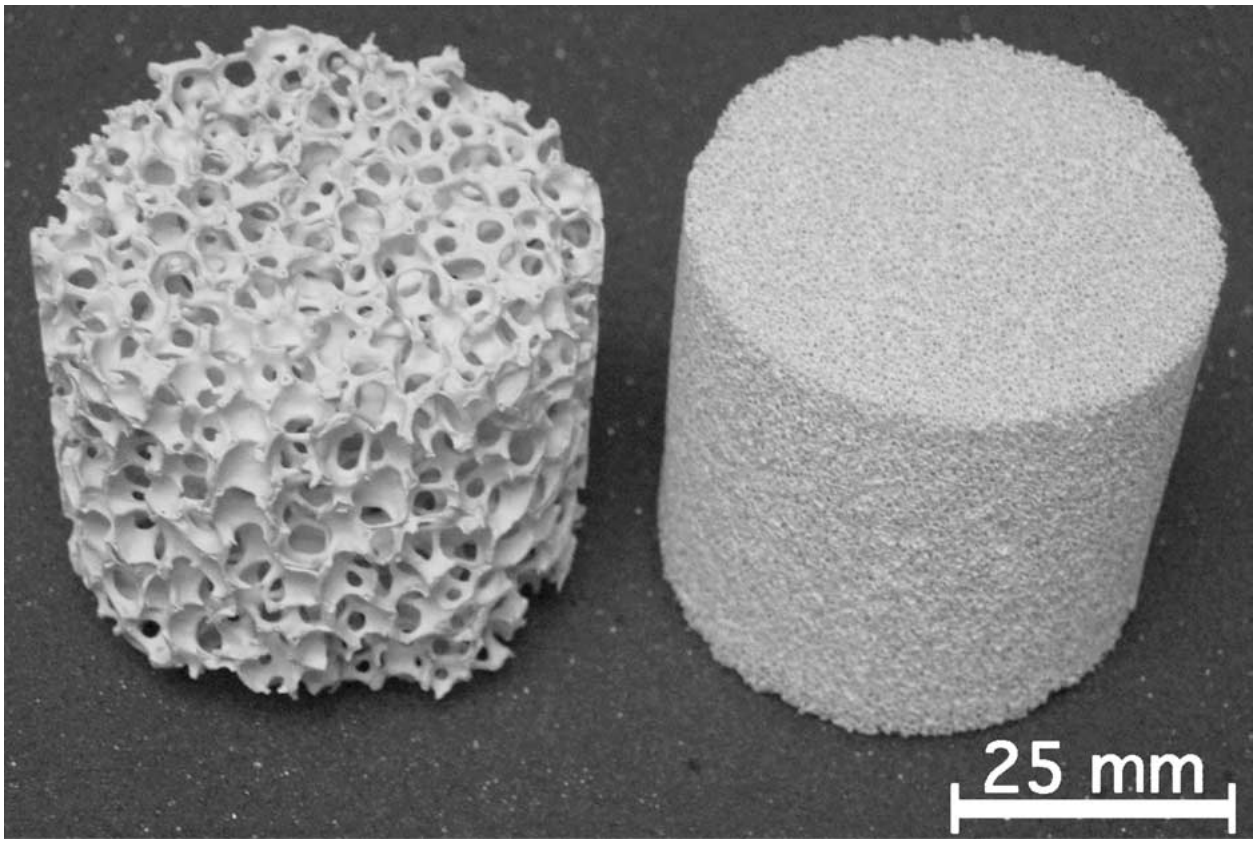

Figure 2 Photograph showing the 3.9 and 23.6 ppc YZA foams.

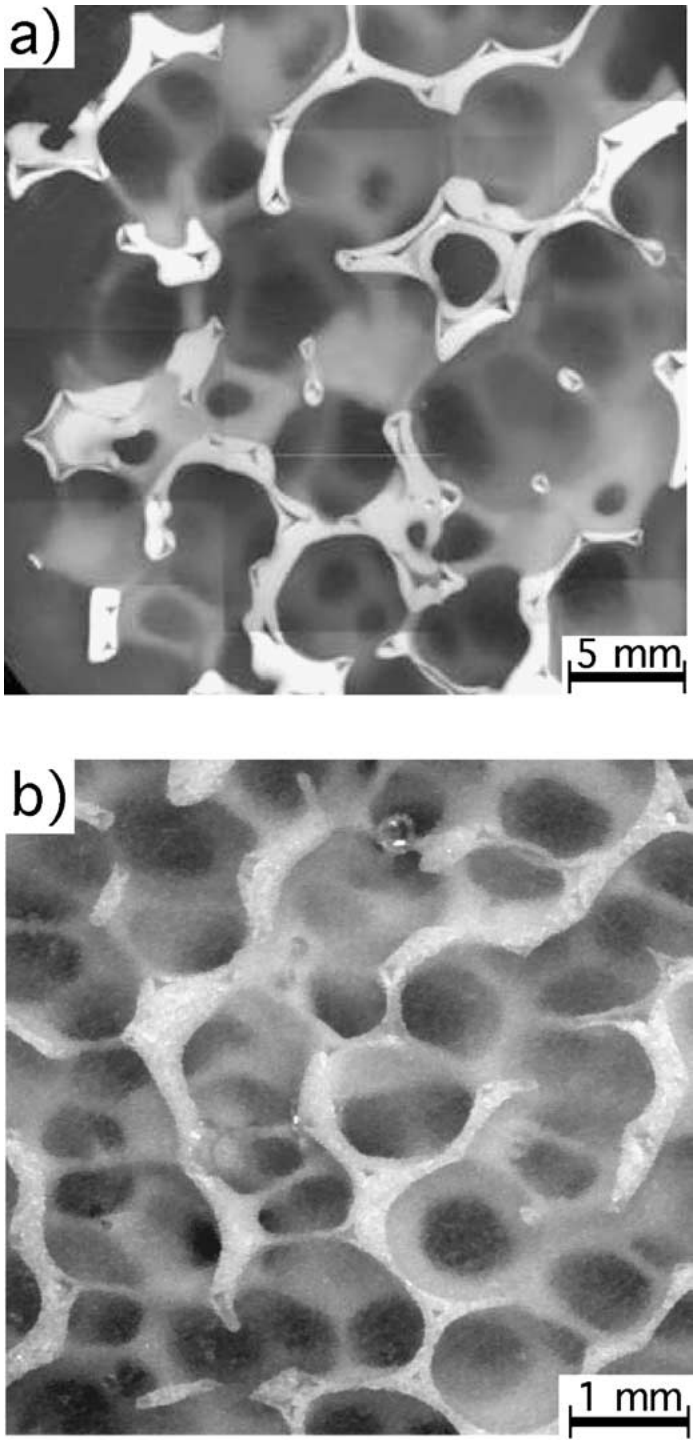

Figure 3 Optical micrographs showing a cross section of (a) the 3.9 ppc and (b) the 23.6 ppc foams. Note the difference in magnifications.

yielded slightly higher values of relative density (12.9 and 15.6% for the 3.9 and 23.6 ppc foams, respectively), but this difference is well within the range of sample-to-sample variation. Fig. 3a–b also show that the each strut contains a closed pore with three sharp cusps. This intrastrut porosity is a result of the manufacturing process and has been discussed in detail previously [15]. Based on the stereographic analysis, about 2% of the total porosity is closed intrastrut porosity and the remainder consists of the open cells between the struts.

EDS analyses of foams in the as-received state revealed that the materials consist primarily of Al, Zr, and O, with a small fraction of Y, Ca, and Si. After burner testing, there was no measurable change in composition in the foams and no additional elements were detected. Results from powder X-ray diffraction revealed that the only crystalline phases that were present in the as-received coupons were α-Al_2O_3, monoclinic ZrO_2, and a smaller fraction of tetragonal ZrO_2. After burner testing, the X-ray diffraction pattern was unchanged, confirming that no chemical reactions had taken place during the burner testing. It should be noted that coupons likely consisted a much greater fraction of tetragonal zirconia but it was not possible to quantitatively determine the relative fractions of monoclinic to tetragonal zirconia in the foams before and after burner testing using this technique because the process of pulverizing the foams to perform diffraction results in transformation

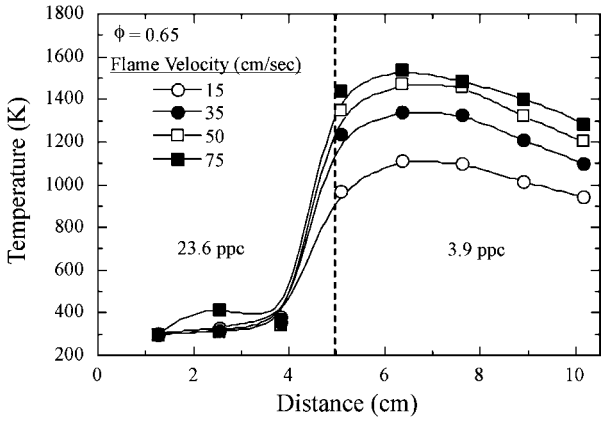

Figure 4 Measured temperature distribution in a burner at $\phi = 0.65$ for different gas flow rates. Each ceramic foam coupon is 5 cm long and the direction of gas flow is from left to right. The 23.6 ppc foam is located on the inlet side and the vertical line denotes the position of the interface between the 3.9 and 23.6 ppc foams.

of a significant fraction of the tetragonal zirconia to monoclinic zirconia.

3.2. Burner testing

Previous experiments have shown that the peak temperature within the burner generally increases as the flow rates or the equivalence ratios are increased [9]. A representative plot of the temperature distribution in the burner for an equivalence ratio of 0.65 is shown in Fig. 4 as a function of flame velocity. The peak temperature under these conditions occurs in the 3.9 ppc foam, just downstream from the interface between the foams. The magnitude of this peak increases with flow velocity, reaching a maximum of about 1500 K at a flow velocity of 75 cm/s. Although the peak temperature in the burner occurs near the upstream surface of the 23.6 ppc foam, the temperature is relatively constant in this area under steady-state conditions and thus the thermal gradient throughout the 23.6 ppc foam is small. In contrast, the temperature gradient in the 3.9 ppc foam is much more severe with a maximum gradient of about 850 K/cm occurring near the interface between the foams.

3.3. Mechanical testing

Compressive strength is plotted for as-received foams and for foams after burner testing in Fig. 5. The average strength for the as-received 3.9 ppc foam is about 1.8 MPa and the average strength for the as-received 23.6 ppc foam is about 2.5 MPa. In both cases, considerable variability in strength is observed. The coupons exposed to burner condition 1 ($\phi = 0.65$, flow velocity = 30 cm/s, $t = 30$ min) do not appear to suffer any measurable degradation in strength relative to the as-received coupons. Coupons exposed to burner condition 2 ($\phi = 0.72$, flow velocity = 40 cm/s, $t = 30$ min) exhibit a moderate strength decrease with the mean strength dropping by 33% compared to the as-received samples for the 3.9 ppc foam and by 40% for the 23.6 ppc foam. Coupons from burner condition 3 ($\phi = 0.70$, flow velocity = 40 cm/s, $t = 240$ min) exhibit similar strengths to those from burner condition

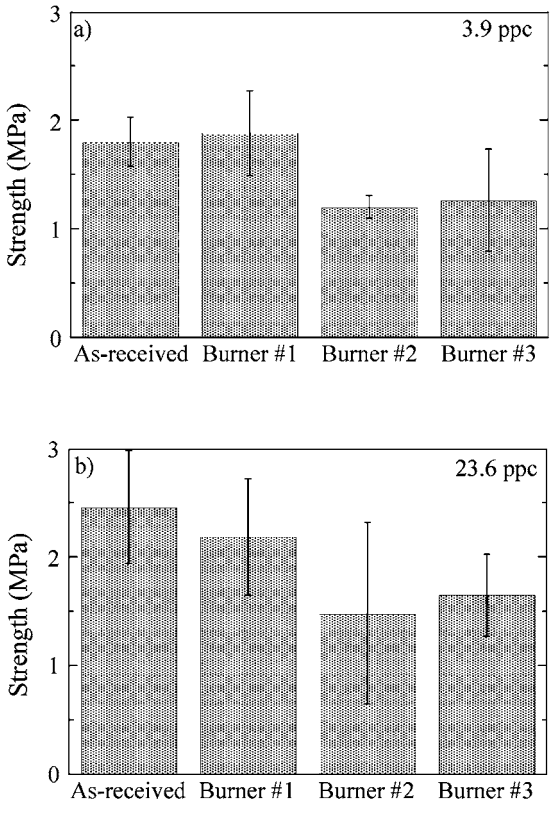

Figure 5 Strength is plotted for as-received coupons and coupons exposed to the burner for (a) 3.9 ppc and (b) 23.6 ppc foams.

2 which indicates that extending the operation time of the burner by a factor of four does not significantly impact the damage introduced into the foams during burner testing.

Results of the water quench tests are shown in Fig. 6. Both the 3.9 and 23.6 ppc foams exhibit a moderate decrease in strength with increasing severity of the thermal quench. The onset of damage occurs in both materials at $\Delta T = 200$–400 K. For $\Delta T = 800$ K, the mean strength of the 3.9 ppc foam is reduced by 38% while for the 23.6 ppc foam the strength is reduced by 56% relative to the as-received foams.

4. Discussion

4.1. Strength of as-received foams

The measured compressive strengths for the two YZA foams in the as-received state were 1.8–3.0 MPa. The compressive strength for YZA foams has not been previously reported in the literature but a bending strength of 1.56–2.05 MPa for YZA foams with similar densities and cell sizes has been reported [16]. Orenstein and Green have shown that there is little difference between the bending and compressive strength of alumina ceramic foams [13].

Based on the model of Gibson and Ashby [17], the compressive strength should be independent of cell size and can be related to the relative density by

$$\sigma_{fc} = C_6 \sigma_{fs} \left(\frac{\rho}{\rho_s} \right)^{3/2} \tag{2}$$

where σ_{fc} is the compressive strength of the ceramic foam, C_6 is a constant, σ_{fc} is the strut strength in

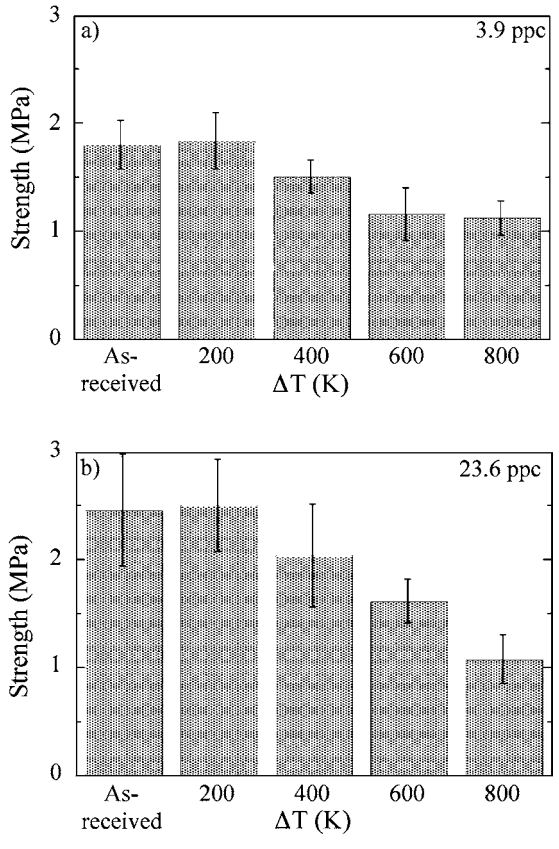

Figure 6 Strength is plotted for as-received coupons and for coupons exposed to a water quench for (a) 3.9 ppc and (b) 23.6 ppc foams.

bending, ρ is the density of the foam, and ρ_s is the density of the struts.

Comparing the compressive strength and correcting for the approximately 2.5% difference in density in between the 23.6 ppc foam and the 3.9 ppc foam, it is clear that differences in density alone cannot account for the 27% difference in the measured compressive strengths in these materials. As discussed by Brezney and Green [18], there are several other possible explanations for this observation but the most likely is that the strut strength, σ_{fs}, in the 3.9 ppc foam is lower than in the 23.6 ppc foam. Similar results have been reported previously in a vitreous carbon foam [18]. These differences have been attributed to differences in the flaw populations within the struts [18].

4.2. Burner tests and quench tests

Examination by EDS and XRD indicated that there was no measurable change in the chemical composition or the crystal structure of the ceramic foams during burner testing. This indicates that degradation in strength in porous burners does not result from chemical changes in the foams but rather results from mechanical damage that occurs during operation of the burner.

Compressive tests on coupons removed from the burner and on coupons exposed to water quenching from high temperature reveal that there are several similarities in the degradation mechanisms that occur during these tests. For coupons removed from the burner or exposed to a water quench, there was a gradual reduction in strength as the severity of the thermal shock was increased, consistent with previous reports for other ceramic foams exposed to a water quench [13]. In this study, the onset of strength degradation caused by water quenching occurred at a critical value of $\Delta T = 200$–400 K in both the 3.9 and 23.6 ppc foams. Similar critical values of ΔT have been reported previously for water quenching of alumina foams, independent of pore size [13]. It has also been reported that for foams exposed to infrared heating to induce temperature gradients, thermal shock resistance increases with cell size [16].

The magnitude of the strength degradation for the water quench tests was greater for the 23.6 ppc foam compared to the 3.9 ppc foam (56% loss of strength versus 38%). In the burner tests, similar behavior was observed but the differences in strength degradation were not as great between the 23.6 and 3.9 ppc foams (40% versus 33%). Comparing results from a previous study on a 4 ppc alumina [13] to the current results, the YZA foams used in this study are considerably more resistant to thermal shock from a water quench. For example, for $\Delta T = 600$ K, the YZA foams retained about 65% of their original strength whereas the alumina foam used in the previous study retained only about 35% of its original strength at the same ΔT. Although the fracture toughness of dense YZA is considerably greater than alumina, the thermal shock resistance of dense YZA and alumina are similar [19, 20]. Thus, it is likely that the differences in strength degradation between foams result from differences in the flaw populations within the struts and the geometry of the cells rather than differences in the intrinsic thermal shock resistance of the strut materials [13].

4.3. Fracture morphology and damage tolerance

Coupons were observed to exhibit one of three distinct fracture morphologies depending on the severity of the thermal shock. Representative photographs showing each of these morphologies are shown in Fig. 7. For coupons in the as-received condition or exposed to modest thermal gradients, damage during compression testing was homogeneously distributed over the surface of the specimen in contact with the loading platen (Fig. 7a), as reported previously [14]. As the magnitude of the thermal gradient was increased by increasing ΔT for the coupons exposed to the water quench or by increasing the gas flow rate and/or equivalence ratio for samples exposed to the burner environment, there was a distinct transition to more localized damage mechanism which has not been reported previously. Compressive loading of these coupons resulted in the propagation of a dominant crack at approximately 45° to the applied loading axis, along the directions of maximum shear stress (Fig. 7b). Further increases in the magnitude of the thermal shock resulted in a second transition. For these samples exposed to very large thermal gradients, damage was localized along an axial plane parallel to the loading axis (Fig. 7c). For coupons that failed by this mechanism, a single crack was observed to propagate through the specimen along this plane with little or no damage to the surface of the coupons. Fig. 8a–b show

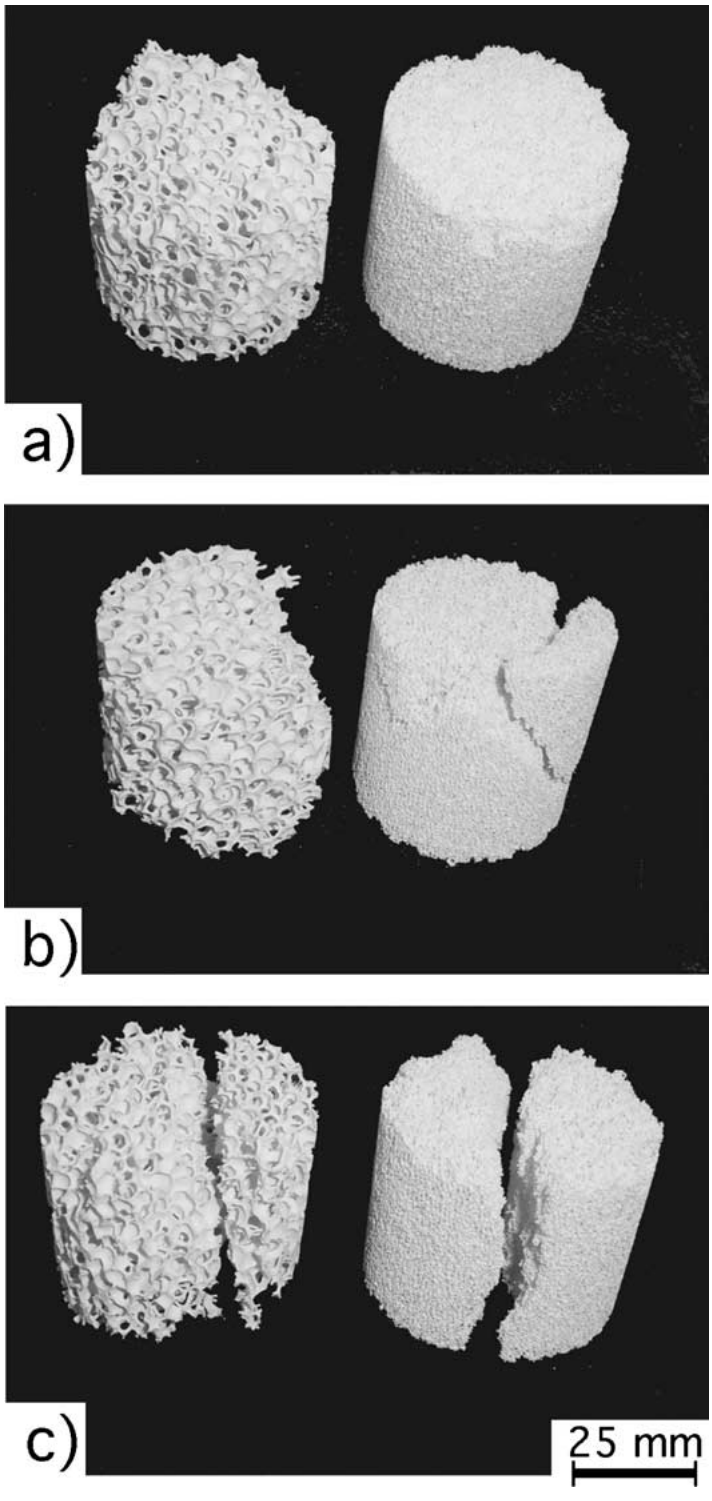

Figure 7 Photographs showing representative coupons observed to fail by (a) homogenous damage of the surface, (b) localized damage along a plane at 45° to the loading axis, and (c) localized damage along an axial plane parallel to the loading axis.

the number of occurrences for each failure mechanism as a function of experimental conditions.

In Fig. 9a–e, engineering stress versus engineering strain is plotted for representative 3.9 and 23.6 ppc foams exhibiting each of the three observed failure modes (surface, shear, and axial). For all of the coupons, an initial non-linearity was observed as the sample contacted the neoprene-lined platens, followed by a linear elastic regime. For the samples where damage was distributed over the surface of the coupons, deviation from the linear regime occurred as individual struts were crushed near the surface. Increases in strain resulted in the gradual evolution of damage along the surface until the peak stress was reached and nearly the entire surface contained fractured struts. Further increases in strain resulted in a gradual reduction in the load bearing capacity of the coupon. Similar behavior was observed in both the 3.9 and 23.6 ppc foam and similar observations have been reported previously during compressive testing of another open celled ceramic foam [14].

For coupons that were observed to fail at approximately 45° to the loading axis, the stress versus strain plots were similar to those exhibiting surface failures

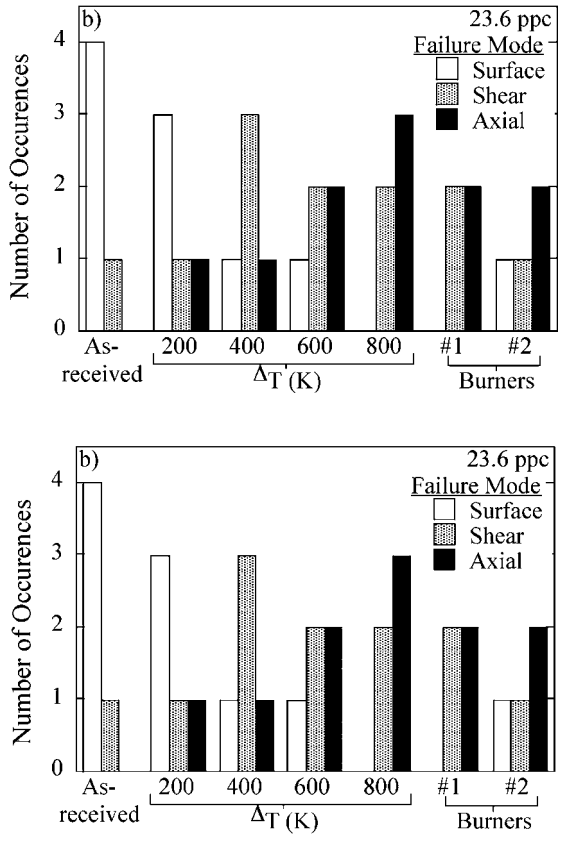

Figure 8 Failure distributions for (a) 3.9 ppc foam and (b) 23.6 ppc foam showing that localized shear or axial failures dominate as the severity of the thermal gradient increases.

except that less damage was observed prior to the peak stress and the reduction in the load bearing capacity occurred more quickly after the peak stress was attained. For coupons that failed by the propagation of a crack parallel to the axis of loading, there was even less damage apparent before the peak stress was reached and the coupons failed nearly catastrophically after the peak stress was obtained. It is interesting to note that the differences in strength between samples failing by these different mechanisms were typically less than a factor of two, despite the large difference in damage tolerance and the distinct change in fracture morphology between the coupons.

The similarities in fracture behavior of the 3.9 ppc foam and 23.6 ppc foam following burner testing can be explained from the steady-state temperature distributions within the burner shown in Fig. 4. These distributions show that, at steady-state, the peak temperature gradient of approximately 850 K/cm exists in the upstream 23.6 ppc foam while there is only a temperature gradient of about 100 K/cm in the 3.9 ppc foam. However, as pointed out earlier, during start-up, the flame is lit on the downstream surface of the 3.9 ppc foam and then propagates completely through the 3.9 ppc foam before stabilizing near the interface between the foams. Thus, although the steady-state temperature distributions in the foams during burner operation are very different, the peak temperature gradient experienced in both foams due to start-up of the burners are

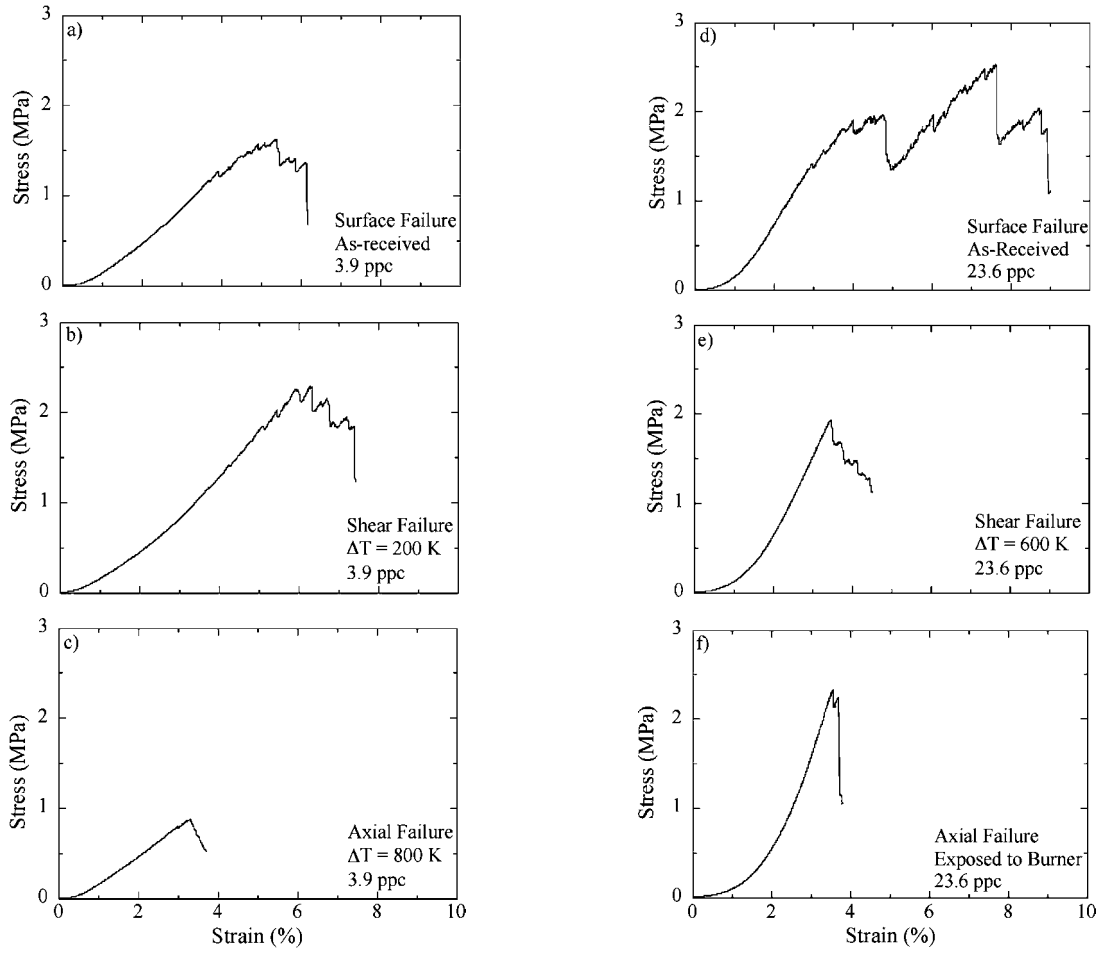

Figure 9 Engineering stress versus engineering strain is plotted for 3.9 ppc foam exhibiting: (a) surface failure, (b) shear failure, (c) axial failure and for the 23.6 ppc foam exhibiting, (d) surface failure, (e) shear failure, and (f) axial failure.

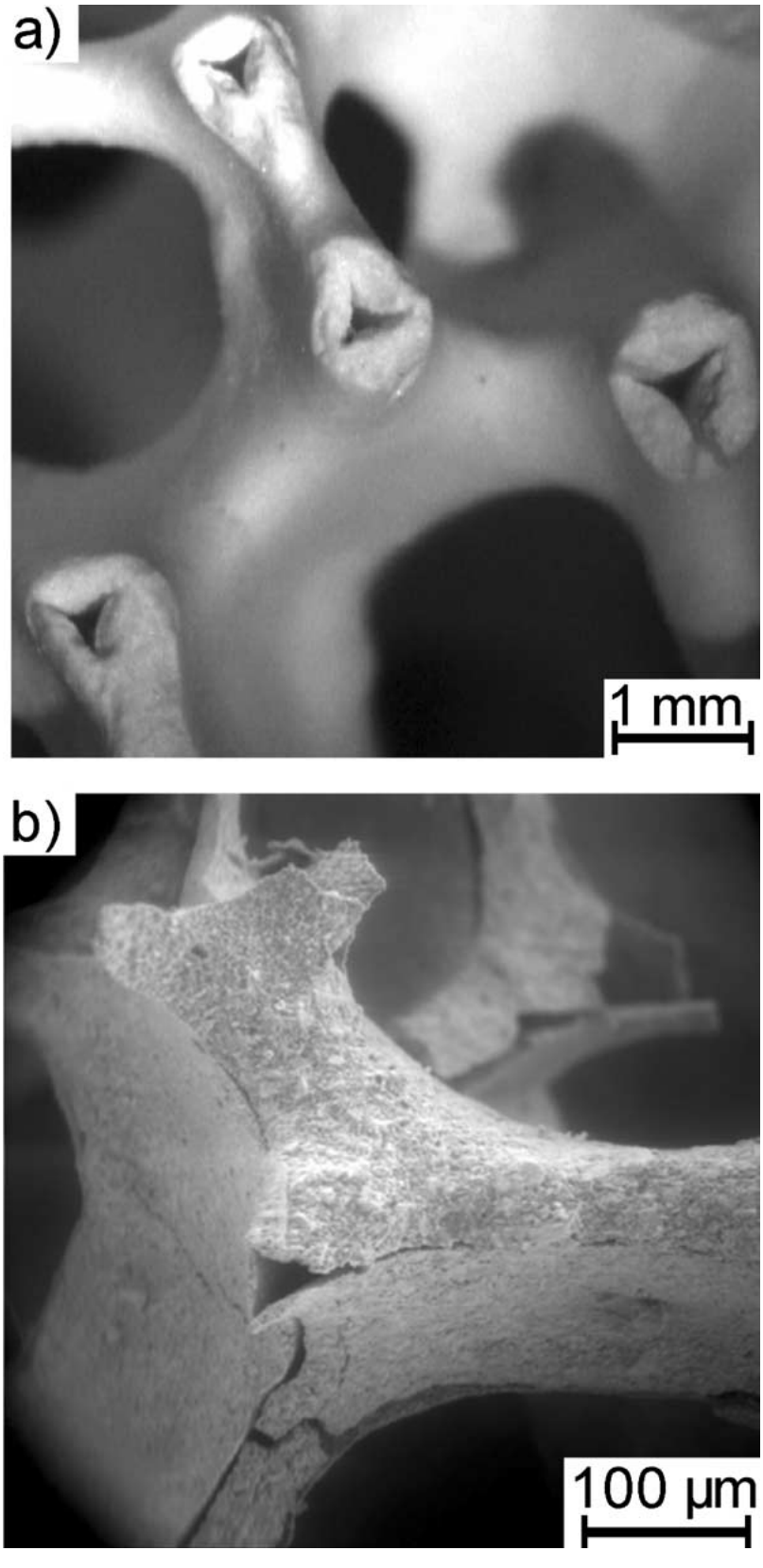

Figure 10 Scanning electron micrograph of (a) cross section of as-received 3.9 ppc coupon showing the presence of intrastrut voids and (b) propagation of cracks from these voids during exposure to the burner.

similar. Recalling that increasing the exposure time in the burner did not influence the strength degradation of the foams, it is apparent that the most of the damage occurs during start-up as a result of these temperature transients.

Fig. 10a is a cross-section of the 3.9 ppc foam in the as-received condition showing that the each strut is hollow containing a pore with three sharp cusps. Other than these intrastrut pores, there are few other defects apparent. Similar observations were made on the 23.6 ppc foam. An SEM micrograph of a the 23.6 ppc foam after quenching and testing shows that the failure mechanisms in this foam involves propagation of cracks from the cusps of the intrastrut pores, splitting of the

struts, and eventually linking of the these cracks until a section of the material fails catastrophically. Similar observations of failure mechanisms in foams have been reported previously in a number of ceramic foams [13, 16].

5. Conclusions

YZA ceramic foams tested in this study suffered less thermal shock damage during water quenching compared to those tested previously under similar conditions and thus are candidate materials for use in porous burners. During burner testing the foams suffered moderate strength degradation as a result of thermal gradients that existed during combustion. The magnitude of the strength degradation was similar in both the 23.6 ppc foam used in the upstream section of the burner and the 3.9 ppc foam used in the downstream section and scaled with the magnitude of the thermal gradients, which in turn varied with gas flow rates and the fuel-to-air ratio. There was no evidence of chemical attack during combustion and increasing the time in the burner did not influence strength. These results suggest that most of the damage to the foams does not occur during steady-state operation of the burner but rather occurs during start-up when transients occur and the maximum thermal gradients likely exist.

Compression tests on coupons removed from burners and on coupons exposed to a water quench revealed a number of similarities in the failure mechanisms. For YZA foams that experienced no thermal gradient or a modest thermal gradient, compression testing resulted in delocalized damage over the entire specimen. Corresponding plots of stress versus strain exhibited significant non-linearity prior to the peak stress and the coupons retained significant load-bearing capacity after the peak stress to large strains. For coupons exposed to large thermal gradients, compression tests resulted in localized failure by propagation of a dominant crack along a plane. The corresponding plots of stress versus strain revealed significantly less non-linearity prior to the peak stress and nearly catastrophic failure with little load bearing capacity after the peak stress. This dramatic change in fracture morphology and retained damage tolerance despite only small differences in strength has not been reported previously and suggests that damage in YZA foams from exposure to large thermal gradients during water quenching or in a porous burner is highly localized.

Acknowledgements

The authors would like to thank Dr. Michael Schmerling for his assistance with the SEM/EDS analysis.

References

1. J. R. HOWELL, M. J. HALL and J. L. ELLZEY, *Prog. Energy Comb. Sci.* **22**(2) (1996) 121.
2. R. VISKANTA and J. P. GORE, *Environ. Comb. Tech.* **1** (2000) 167.
3. T. TAKENO and K. SATO, *Comb. Sci. Tech.* **20** (1979) 73.
4. Y. KOTANI and T. TAKENO, in "Ninteenth Symposium (International) on Combustion" (The Combustion Institute, Pittsburgh, PA, 1986) p. 1503.
5. S. B. SATHE, M. R. KULKARNI, R. E. PECK and T. W. TONG, in "Twenty-Third Symposium (International) on Combustion" (The Combustion Institute, Pittsburgh, PA, 1990) p. 1011.
6. V. KHANNA, R. GOEL and J. L. ELLZEY, *Comb. Sci. Tech.* **99** (1994) 133.
7. D. P. HAACK, "Application of Reticulated Ceramic Foam to Radiant Burners," Vol. I, Gas Research Institute report #GRI-96/0255.1, 1997.
8. P.-F. HSU, W. D. EVANS and J. R. HOWELL, *Comb. Sci. Tech.* **90**(1–4) (1993) 149.
9. W. M. MATHIS, P. J. ELVERUM and J. L. ELLZEY, in Proceedings of the Spring Meeting of the Western States Section of the Combustion Institute (La Jolla, CA, 2002).
10. K. C. GORETTA *et al.*, *Mater. Sci. Eng.* A **124** (1990) 151.
11. R. BREZNY and D. J. GREEN, *J. Amer. Ceram. Soc.* **72**(7) (1989) 1145.
12. P. J. ELVERUM, J. L. ELLZEY and D. KOVAR, in Proceedings of the Spring Meeting of the Western States Section of the Combustion Institute (La Jolla, CA, 2002).
13. R. M. ORENSTEIN and D. J. GREEN, *J. Amer. Ceram. Soc.* **75**(7) (1992) 1899.
14. C. Q. DAM, R. BREZNY and D. J. GREEN, *J. Mater. Res.* **5**(1) (1990) 163.
15. D. D. BROWN and D. J. GREEN, *J. Amer. Ceram. Soc.* **77**(6) (1994) 1467.
16. V. R. VEDULA, D. J. GREEN and H. JOHN R, *ibid* **82**(3) (1999) 649.
17. L. J. GIBSON and M. F. ASHBY, "Cellular Solids: Structure and Properties" (Pergamon Press, Oxford, England, 1988).
18. R. BREZNY and D. J. GREEN, *Acta Metall. Mater.* **38**(12) (1990) 2517.
19. T. K. GUPTA, *J. Amer. Ceram. Soc.* **55**(5) (1972) 249.
20. M. ISHITSUKA, T. SATO, T. ENDO and M. SHIMADA, *J. Mater. Sci. Lett.* **24** (1989) 4057.

Received 20 August 2003
and accepted 25 August 2004